THE JOURNAL OF PHYSICAL CHEMISTRY C

Article

Cite This: J. Phys. Chem. C 2017, 121, 27555−27562

pubs.acs.org/JPCC

Transitions in Al Coordination during Gibbsite Crystallization Using High-Field ^{27}Al and ^{23}Na MAS NMR Spectroscopy

Jian Zhi Hu,*[†,§] Xin Zhang,[†,§] Nicholas R. Jaegers,[†,‡,§] Chuan Wan,[†,§] Trent R. Graham,[†,‡,§] Mary Hu,[†] Carolyn I. Pearce,[†] Andrew R. Felmy,[†,‡] Sue B. Clark,[†,‡] and Kevin M. Rosso*[,†]

[†]Pacific Northwest National Laboratory, Richland, Washington 99354, United States

[‡]Washington State University, Pullman, Washington 99164, United States

Supporting Information

ABSTRACT: Mechanisms of nucleation and growth of Al hydroxides such as gibbsite from aqueous solution, particularly in highly alkaline conditions, remain poorly understood. In this work, quantitative ^{27}Al and ^{23}Na MAS NMR experiments were conducted on solid samples extracted from the crystallization of gibbsite from an amorphous aluminum hydroxide gel precursor. The use of a high magnetic field and a moderate sample spinning rate of 20 kHz allowed transitional tetrahedral (Al_T) and pentahedral (Al_P) aluminum species to be observed along with the octahedral aluminum (Al_O) that dominates the gibbsite product. Low-coordinated Al species could be detected at concentrations as low as 0.1% of the total Al sites. The following results have been established: (a) Al_T and Al_P coexist on the surface of growing gibbsites even with a combined percentage over the total Al sites of less than 1%. (b) Different synthesis methods generate gibbsite with varying amounts of low-coordinated Al. (c) The amorphous gel precursor contains a significant amount of low-coordinated Al sites with an Al_O:Al_P:Al_T ratio of approximately 4:2:1. (d) Upon hydration, the external, low-coordinated Al sites become 6-fold coordinated by interacting with the oxygen in H_2O, and the ^{27}Al MAS NMR peak position shifts to that for the Al_O sites. (e) Gibbsite with increased long-range order is synthesized over longer times by gradually incorporating residual Al_P and Al_T sites into octahedrally coordinated Al_O sites. (f) Trace Na is predominantly a surface species on gibbsite particles. These findings provide a basis for understanding the gibbsite crystallization mechanism, along with a general means of characterizing gibbsite surface properties that are of equal importance for understanding related processes such as dissolution behavior.

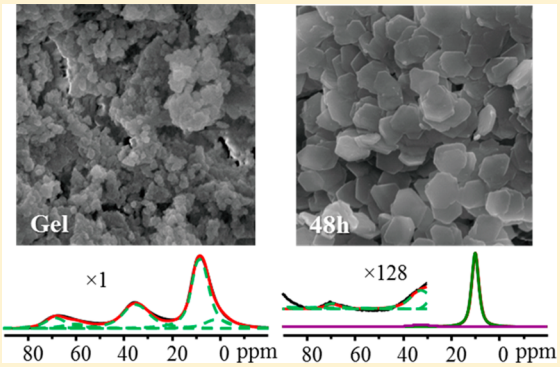

INTRODUCTION

Understanding nucleation and growth of aluminum hydroxide minerals from aqueous solution is of long-standing basic and applied interest. For example, under highly alkaline conditions, nucleation appears to be highly inhibited for reasons that remain poorly understood. In the aluminum processing industry, precipitation of α-$Al(OH)_3$ (gibbsite) from Bayer liquors often requires seed crystals to overcome an apparent energy barrier.[1−3] At these high-pH conditions, precipitation involves an essential change in Al^{3+} coordination from tetrahedral in soluble aluminate to octahedral in gibbsite. However, the extent to which coordination change is coupled to the activation energy for nucleation is difficult to probe.

Analogous considerations also apply in the processing of vast quantities of radioactive high-level waste (HLW) stored at the Hanford Nuclear Reservation (Hanford, WA).[4] Aluminum was introduced into the HLW in a variety of chemical forms, including as fuel cladding, as ionic additives for separations, and as fluoride corrosion inhibitors.[5] Sodium hydroxide (NaOH), added to increase pH for mitigation of tank corrosion, resulted in solubilization of the Al in the form of sodium aluminate ($NaAlO_4$). Subsequent precipitation of the Al occurred as a result of changes in NaOH concentration, temperature, etc. Gibbsite and γ-AlOOH (boehmite) are two of the most common solid precipitated phases present.[6] Techniques to retrieve HLW from tanks leave residual solids containing significant amounts of gibbsite contaminated with uranium-238, chromium, iodine-129, and technetium-99.[7] Concerns regarding excess or unintentional gibbsite precipitation relate to the need to dilute the concentrated aqueous NaOH waste stream containing large concentrations of dissolved Al prior to vitrification at the waste treatment plant (WTP) and include the potential for clogging transfer lines, fouling of ion−ion exchangers,[6] and detrimental effects on HLW vitrification.[8] Thus, techniques that can probe the changes in Al coordination from tetrahedral to octahedral and vice versa at the solid interfaces with these caustic solutions would be useful for understanding and predicting transformation kinetics.

The present study focuses on developing this ability to characterize transitions in Al coordination at gibbsite surfaces as

Received: October 21, 2017
Revised: November 13, 2017
Published: November 15, 2017

DOI: 10.1021/acs.jpcc.7b10424
J. Phys. Chem. C 2017, 121, 27555−27562

a function of growth conditions. The interfacial reactivity of gibbsite is governed by the structure and coordination of Al at specific crystallographic surfaces.[9] Gibbsite is composed of pairs of close-packed hydroxyl layers in which aluminum cations occupy two-thirds of the octahedral interstices (Al_O) to form an $Al(OH)_3$ sheet and sheets are connected and stacked along the basal direction through interlayer hydrogen bonds.[10] Stable gibbsite edge terminations include the (110), (010), and (100) faces;[11,12] these are typically the fast-growth directions, yielding a tabular morphology with a dominant (001) basal surface. The distribution of aluminum coordination includes tetrahedral (Al_T)[13] and pentahedral (Al_P) species expectedly concentrated at the edge surfaces,[14,15] with Al_P hypothesized to be a transitional intermediate species between Al_T and Al_O. These lower coordinated aluminum sites are nominally the active sites during growth and dissolution.[16−18]

A powerful technique for investigating Al coordination is ^{27}Al magic-angle spinning nuclear magnetic resonance (MAS NMR) spectroscopy.[19] ^{27}Al is a favorable nucleus for NMR spectroscopy due to its high natural abundance (effectively 100%) and short relaxation times. However, as a spin $^5/_2$ nucleus, it is subject to nuclear quadrupole moment interaction with the electron field gradient, causing a concomitant broadening and distortion of the NMR spectrum.[20] Utilization of high-field and moderate spinning rates is necessary to resolve different aluminum coordination states. Previous ^{27}Al MAS NMR studies have shown that exposing gibbsite to mechanochemical stress increases the composition of Al_T and Al_P at the expense of Al_O.[21] Mixtures of Al_T, Al_P, and Al_O coordination sites in aluminum hydroxide nanoparticles prepared by laser ablation have also been characterized by ^{27}Al NMR spectroscopy.[22] The occurrence of the Al_P and Al_T in gibbsite appears inversely related to its crystallinity.[14] The addition of surfactants to crystalline gibbsite converts a significant portion of Al_O coordinated aluminum to Al_T through an unexplained mechanism.[23] Despite these various observations of aluminum coordination in gibbsite, there exists no systematic investigation into the effects of the gibbsite synthesis conditions on the distribution and location of aluminum coordination sites.

In this study, we use MAS NMR spectroscopy to investigate Al coordination during gibbsite nucleation and growth from a hydrous colloidal amorphous gel precursor in the presence of sodium hydroxide at mild hydrothermal conditions. The use of ultrahigh fields enables clear resolution of low-coordinated aluminum sites. We detect trace amounts of Al_P and Al_T and provide insight into the dynamics of Al coordination during gibbsite growth. We conduct complementary ^{23}Na MAS NMR to investigate the changes in Na content throughout gibbsite growth. While ^{23}Na MAS NMR has been used previously to describe the precipitation of gibbsite from acidic solutions,[24] the role of Na during the transformation studied here is less understood. This work advances our understanding of the distribution of aluminum coordination sites during gibbsite growth and begins to provide insight into mechanisms of transformations in play during HLW processing.

EXPERIMENTAL METHODS

Amorphous Gel to Gibbsite Transformation. Samples were prepared using a hydrothermal synthesis method. Typically, $Al(NO_3)_3{\cdot}9H_2O$ (≥98%, Sigma-Aldrich) was dissolved into deionized water to form a homogeneous solution with a concentration of 0.25 M at room temperature. The addition of 1 M NaOH (≥98%, Sigma-Aldrich) aqueous solution adjusted the pH to around 5.0. The mixture was continuously stirred for 1 h, and then the solution was centrifuged to collect a gel-like precipitate. The gel was washed with deionized water three times to form the sample delineated as G0. Al gels (0.5 M) were dispersed in deionized water, and the suspension (16 mL) was transferred to a 20 mL Teflon autoclave. The Teflon autoclave was sealed into a Parr bomb and heated in an electric oven at 80 °C for 12, 24, 48, and 72 h to prepare samples G1, G2, G3, and G4, respectively. The resulting white product was recovered by centrifugation and washed with deionized water (DIW) three times. Dehydrated versions of the as-synthesized hydrated materials were prepared by drying samples in an oven at 50 °C and 10^{-2} Torr until the sample mass no longer changed.

Conditions for Additional Specific Gibbsite Samples. Sample G5 was prepared by using the $Al(OH)_3$ gel.[25] $Al(NO)_3$ (40 g) was dissolved in DIW (800 mL) with stirring to form a homogeneous solution at room temperature. An aqueous ammonium hydroxide solution (10 wt %) was used to adjust the pH to ∼5.0. After continuous stirring for 1 h, the suspension was centrifuged and the precipitated gel-like material (80 mL) was transferred to 100 mL Teflon autoclaves. The Teflon autoclaves were then sealed into Parr bombs and heated in an electric oven at 100 °C for 10 d.

Sample G6 was prepared using the same procedure as for G4, but the gel concentration was 0.75 M.

Sample G7 was prepared using an organic precursor.[26] Aluminum *sec*-butoxide (ASB, >97%, 25.6 mmol) was added to an aqueous HCl solution (0.05 M, 800 mL) and stirred for 18 h at room temperature. The solution was then heated to 50 °C for 6 h, and the resulting solution (80 mL) was transferred to a 100 mL Teflon autoclave. The Teflon autoclave was sealed within a Parr bomb and heated in an electric oven at 80 °C for 5 d. After the autoclave cycle, the products were recovered by centrifugation and washed with DIW five times. The obtained solid sample was dried in an oven at 80 °C overnight.

NMR Analysis. Single-pulse ^{27}Al MAS NMR experiments were performed at room temperature (∼20 °C) on a Varian-Inova 850 MHz NMR spectrometer using a commercial 3.2 mm pencil-type probe and operating at a magnetic field of 19.975 T and sample spinning rate of 20 kHz. The corresponding ^{27}Al and ^{23}Na Larmor frequencies were 221.413 and 224.768 MHz, respectively. For ^{27}Al MAS NMR acquisitions, a single pulse sequence with a pulse width of 0.5 μs (corresponding to a solid $^{\pi}/_4$ pulse) and ^{27}Al radio frequency (rf) field strength of 83.3 kHz [i.e., 3.0 μs for liquid $^{\pi}/_2$ calibrated by using 1 M $Al(NO_3)_3$ aqueous solution] was used. Each spectrum was acquired using a recycle delay time of 1 s, which is sufficiently long to allow all the magnetization returning to the equilibrium state [see Figure S1 calibration in the Supporting Information (SI)], and an acquisition time of 20 ms. Chemical shifts were referenced to 1 M $Al(NO_3)_3$ aqueous solution (0 ppm). Both hydrated and dehydrated ^{27}Al MAS NMR spectra were collected with 3000 scans.

For ^{23}Na MAS NMR, a single pulse sequence with a pulse width of 0.8 μs (corresponding to a solid $^{\pi}/_4$ pulse) and ^{23}Na radio frequency (rf) field strength of 83.3 kHz (i.e., 3.0 μs for liquid $^{\pi}/_2$ calibrated by using 1 M NaCl aqueous solution) was used. ^{23}Na chemical shifts were referenced to an aqueous NaCl solution (0 ppm), and 1600 scans were acquired for each ^{23}Na MAS spectrum for the hydrated samples. Dehydrated ^{23}Na samples and both hydrated and dehydrated ^{27}Al MAS NMR spectra were collected with 3000 scans. For all of the spectra, a

DOI: 10.1021/acs.jpcc.7b10424
J. Phys. Chem. C 2017, 121, 27555−27562

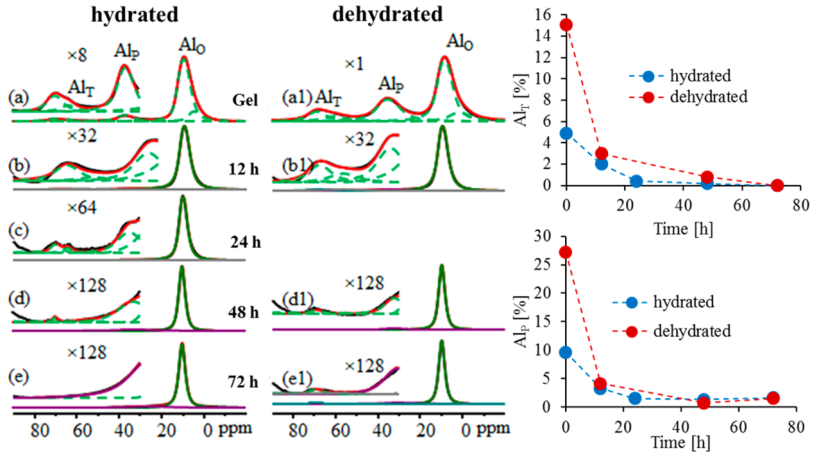

Figure 1. (Left) ^{27}Al MAS NMR spectra of the hydrated (a–e) and the dehydrated (a1, b1, d1, e1) solid samples from the conversion of gel to gibbsite. Intensity scaling relative to the Al_O intensity is noted. The gel (G0) is visible in spectra a and a1, the 12 h product sample (G1) is visible in spectra b and b1, the 24 h product sample (G2) is visible in spectrum c, the 48 h product sample (G3) is visible in spectra d and d1, and the 72 h product sample (G4) is visible in spectra e and e1. The quadrupolar line shape simulated ^{27}Al MAS NMR spectra using our previously reported methods[27,30] are superimposed on top of the experimental spectra. The simulated quadrupolar coupling constants, the line broadening, and the isotropic chemical shifts are provided in the Supporting Information (Table S2). (Right) The relative percentages of the tetrahedral-Al (Al_T) and the pentahedra-Al (Al_P) over the total integrated Al signal as a function of the synthesis time are displayed on the top and bottom, respectively.

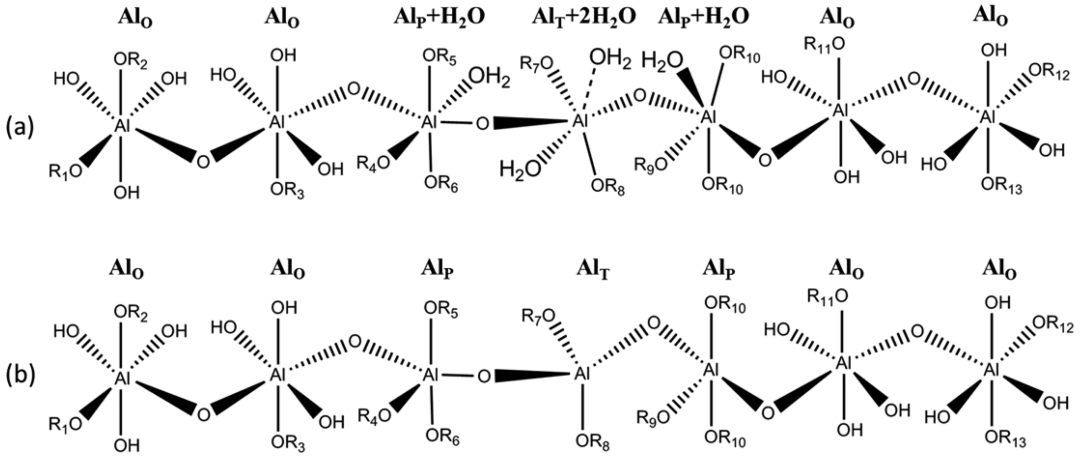

Figure 2. A hypothetical model for the amorphous gel, where R_1, R_2, R_3, R_{11}, R_{12}, and R_{13} represent an oxygen bond to Al in an alumina network of a similar kind and R_4, R_5, R_6, R_7, R_8, R_9, and R_{10} are either H or Al in an alumina network. Here the units of Al_T and Al_P are shown in the middle of the structural unit, but they can be at any location, including the chain ends, resulting in different conformers of the model structure. These variants may be the reason why for some peaks more than one quadrupolar line shape is needed to fit each Al environment in Figure 1. (a) The as-synthesized gel with the minimum hydration that is required to make both the Al_T and Al_P sites coordinated by six oxygens. (b) The dehydrated gel where the coordinated water molecules have desorbed from the tetra- and pentahedral Al sites.

line broadening of 50 Hz was applied before Fourier transformation.

X-ray Diffraction (XRD) Analysis. XRD patterns of the samples were recorded on a Philips X'pert multipurpose diffractometer (MPD) (PANAlytical, Almelo, The Netherlands) equipped with a fixed Cu anode operating at 45 kV and 40 mA. XRD patterns were collected in the 5°–60° 2θ-range. Phase identification was performed using JADE 9.5.1 from Materials Data Inc. and the 2012 PDF4+ database from the International Center for Diffraction Data (ICDD) database.

Scanning Electron Microscopy (SEM) Analysis. The morphologies of as-prepared samples were examined by a Helios NanoLab 600i SEM (FEI, Hillsboro, OR). All samples were sputter-coated with a thin layer of carbon (~5 nm) to ensure conductivity for imaging.

RESULTS AND DISCUSSION

^{27}Al MAS NMR. Figure 1 shows the center band ^{27}Al MAS NMR spectra for both hydrated and mildly dehydrated samples, corresponding to spectra acquired from the initial state (gel in Figure 1a) to progressively longer synthesis times (12–72 h, G1–G4 in Figure 1b–e). The spectrum of hydrated gel (G0 in Figure 1a1) is comprised of three major peaks located at about 9.2, 37.3, and 69.6 ppm. On the basis of our prior high-field ^{27}Al MAS work on transitional Al oxides with medium to high surface areas, in particular for γ-Al_2O_3,[27–29] these peaks are assigned to Al_O, Al_P, and Al_T sites, respectively. Both the Al_P and Al_T are low-coordinated Al sites that reside on surfaces.

It is interesting to note that the relative percentages of both Al_T and Al_P are increased by a factor of 3 after dehydration of the gel sample (G0). Considering that the absolute total peak area of the spectrum, scaled to per unit weight of sample, for

DOI: 10.1021/acs.jpcc.7b10424
J. Phys. Chem. C 2017, 121, 27555–27562

the hydrated sample is about 87% that of the dehydrated sample, several conclusions can be drawn. In the hydrated state gel, water molecules on the gel surface adsorb to low-coordinated Al_T and Al_P sites to make both sites appear similar to Al_O sites in the polymeric gel structure, thus adding ^{27}Al peak intensity to the Al_O site positions with concurrent suppression of the Al_T and Al_P signals. After dehydration at 50 °C for 12 h, most, if not all, of the surface-bonded water molecules are removed by desorption, exposing surface Al_T and Al_P sites and allowing their observation in the ^{27}Al MAS NMR spectrum of the dehydrated gel. The fact that there are Al_T and Al_P sites observed even in the hydrated gel sample suggests that some sites (~33%) are not available for coordination with water molecules. It is likely that these inaccessible sites occur at the end of short Al_O polymer chains that aggregate to form gel particles.

With respect to the conversion process, a "surface-inward" mechanism for gibbsite crystallization is then apparent, as the accessible low-coordinated surface sites are consumed first, and by the time of the first sampling point (12 h), both hydrated and dehydrated samples contain the same amount of Al_P and Al_T sites. The relatively inaccessible low-coordinated sites then react over longer time periods. A model can be proposed for the gel with a ratio Al_O:Al_P:Al_T of approximately 4:2:1 based on the Al ratios obtained from the dehydrated samples, where each Al_O site has three −OH groups, each low-coordinated Al_P site is missing one −OR group, and each Al_T site is missing two −OR (where R is either H or Al). At saturated hydration, each Al_P site must coordinate with one H_2O through the oxygen in H_2O, while each Al_T site must coordinate with two H_2O molecules via the oxygens.

A representative model is depicted in Figure 2 to highlight these findings. Figure 2a depicts the water coordination to the otherwise low-coordinated Al centers in the as-synthesized gel. This shows that hydration is required to make both the Al_T and Al_P sites coordinated to six oxygen atoms. It should be mentioned that not all of the Al_P and Al_T sites interact with H_2O, as these species are still observed in the hydrated sample, but at dilute concentrations relative to the dehydrated gel. Figure 2b shows a potential bonding scheme for the dehydrated material given the model for the hydrated gibbsite where the tetra- and penta-coordinated Al sites are more prevalent.

During the crystallization of gibbsite, the half line width of the ^{27}Al NMR peak for Al_O progressively decreases as a function of the reaction time and levels off after 48 h, as shown in Figure 1. The increased line width for the dehydrated gel and 12 h sample compared with their hydrated counterparts is a consequence of decreased Al site symmetry upon removing the surface-bound water, a common phenomenon that has been observed previously in ^{27}Al MAS NMR spectra of dehydrated zeolite.[31] The decrease in Al_O line width as a function of the crystallization time is accompanied by a dramatic decrease of both the Al_T and Al_P sites [see Table S1 (SI) for details]. This decrease in line width further indicates the formation of a lattice structure with increasing long-range order.

As shown in Figure 3, XRD performed on this series of samples showed no diffraction peaks in the pattern for the hydrated gel (Figure 3a), indicating that within detection limits it is amorphous. XRD results show that gibbsite was forming even for the shortest reaction time sample, i.e., at a synthesis time of 12 h (Figure 3b), although the yield at this point was less than 10%, and intensified through 24 h (Figure 3c). Well-ordered highly crystalline gibbsite was observed when the

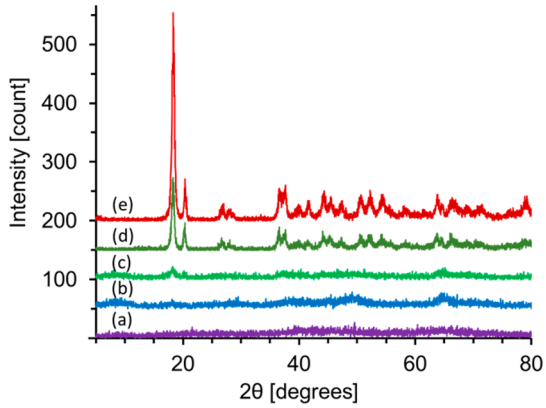

Figure 3. XRD patterns of original $Al(OH)_3$ gel (a) and its transformation to gibbsite at different reaction times of (b) 12 h, (c) 24 h, (d) 48 h, and (e) 72 h.

reaction time exceeded 48 h (Figure 3d), and when the reaction time reached 72 h (Figure 3e), the yield of this material surpassed 80%. We demonstrate that the XRD pattern of the synthesized gibbsite is well-fit by simulated curves using the standard powder diffraction of gibbsite, as shown in Figure S3 (SI).

Scanning electron microscopy (SEM) images show an irregular nanoparticle morphology for the pure gel (Figure 4a), but in all subsequent samples a nanoplate morphology of hexagonal gibbsite was observed (Figure 4b,c), with sizes that matured to between 200 and 400 nm after 24 h of reaction time (Figure 4d,e).

Taken collectively, the results from ^{27}Al MAS NMR, SEM, and XRD suggest that gibbsite, with gradually increasing long-range order, nucleates and grows through conversion of the low-coordinated Al_P and Al_T sites in the amorphous gel into the Al_O sites that comprise α-$Al(OH)_3$. The elimination of coordinatedly undersaturated Al sites approaches an equilibrium limit as synthesis time nears 48 h, evidenced by the 48 and 72 h samples containing a similar abundance of Al_P and Al_T sites (0.8 and 1.7%, respectively).

To determine whether these low-coordinated Al sites are inherent for gibbsite generally, or instead a result of this specific crystallization protocol, additional gibbsite samples synthesized by alternative methods were investigated. The ^{27}Al MAS NMR results are shown in Figure 5a−c, with fitting parameters given in Table S3 (SI). In all of cases, Al_T and Al_P sites are found to coexist with the gibbsite product at a trace abundance of less than 3%. It is reasonable to assume that these under-coordinated Al species are defect sites inherent to gibbsite.

Conceptually, their specific abundance could be related to the different growth kinetics associated with the various synthesis protocols and thus be more intrinsic to the gibbsite bulk, or the average particle size that results, and thus be more intrinsic to the gibbsite surface. In an attempt to resolve this aspect, we tabulated the measured Al site distribution as a function of surface-to-volume ratio, which revealed the following: (i) no clear correlation with Al_T site abundance (Figure 5d), (ii) a systematic decrease in Al_P site abundance with increasing surface-to-volume ratio before dehydration, and (iii) a systematic increase in Al_P site abundance with increasing surface-to-volume ratio after dehydration (Figure 5e). This is consistent with the Al_P sites observed under dehydrated conditions being located on the surface of the nanoparticles and with the Al_P sites resolved in hydrated conditions being

DOI: 10.1021/acs.jpcc.7b10424
J. Phys. Chem. C 2017, 121, 27555−27562

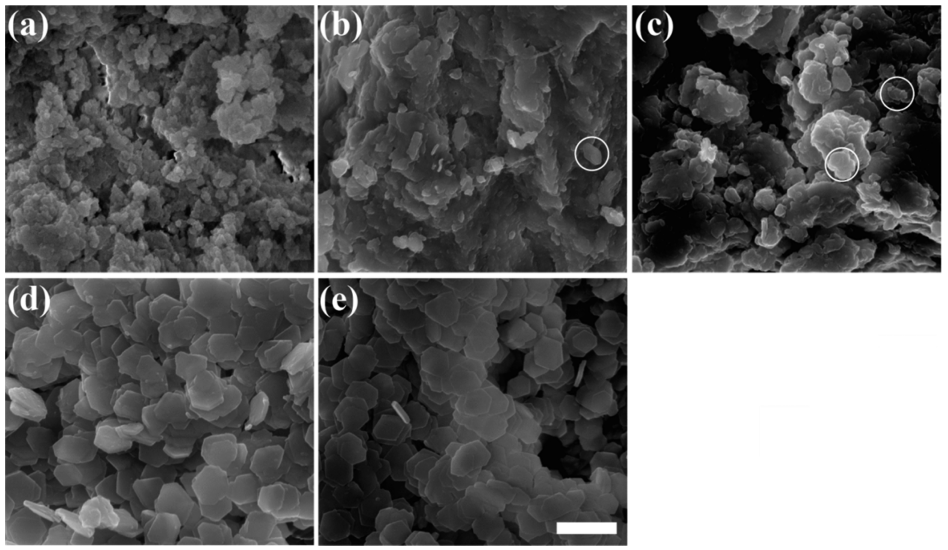

Figure 4. SEM images of (a) original $Al(OH)_3$ gel and the transition into gibbsite at the examined reaction times of (b) 12 h, (c) 24 h, (d) 48 h, and (e) 72 h. Scale bar (inset): 500 nm. The circles in panels b and c highlight the early formation of the hexagonal gibbsite nanoplates.

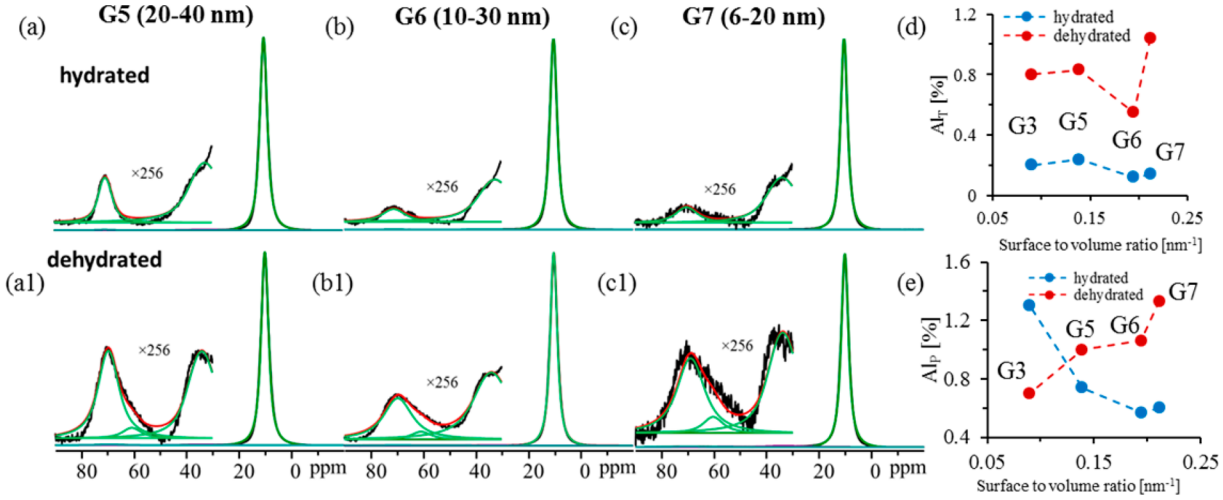

Figure 5. Comparison of the quadrupolar line shape simulated 1D ^{27}Al MAS NMR spectra of gibbsite samples with various particle sizes synthesized by three different protocols (a–c). The green lines indicate deconvoluted peaks, red lines indicate their summation, and solid black lines are experimental spectra. The site distribution of tetra-coordinated Al and penta-coordinated Al sites are shown in panels d and e as a function of the surface to volume ratio.

located at the end of short Al_O polymer chains in the interior of the nanoparticles. The results suggest that smaller gibbsite nanoparticles have a greater population of Al_T and Al_P sites generally, but without being able to fully account for possible differences in crystallinity or nanoporosity within the gibbsite platelets.

^{23}Na MAS NMR. The retention of sodium on the gibbsite product during the transformation from amorphous gel was also investigated, using ultra-high-field ^{23}Na MAS NMR spectroscopy. Figure 6 shows ^{23}Na MAS NMR spectra of both the hydrated (Figure 6a–e) and the dehydrated (Figure 6a1–e1) samples extracted during crystallization at various reaction times. As the reaction time increases, the amount of Na associated with the gibbsite product decreases. The FWHM (full-width at half-maximum) and chemical shift of these Na species were plotted as a function of time (Figure 6f,g). To gain further insight into the role of Na cations, ^{23}Na spin counting experiments were conducted to estimate the number of Na cations per unit weight of sample, following a procedure given in the Supporting Information (Table S4). The resulting concentration of Na cations per milligram of sample for both the hydrated and the dehydrated samples as a function of reaction time is plotted in Figure 6h. Clearly, the gel contains the largest Na concentration per unit weight of sample, and with increasing synthesis time, the Na cation content systematically decreases. The slight increase in Na content per unit mass in dehydrated samples at longer reaction times is due to the loss of water.

Similar to considerations for the under-coordinated Al sites, it is of interest to resolve the question of whether the Na content is a compositional defect component in the gibbsite bulk or if it is associated with the gibbsite surface. If Na cations are in the bulk structure, such as a trapped interstitial species, at a constant trace concentration the total number of Na cations per unit mass would not change with the particle size of the gibbsite. The observed trend of decreasing Na concentration

DOI: 10.1021/acs.jpcc.7b10424
J. Phys. Chem. C 2017, 121, 27555–27562

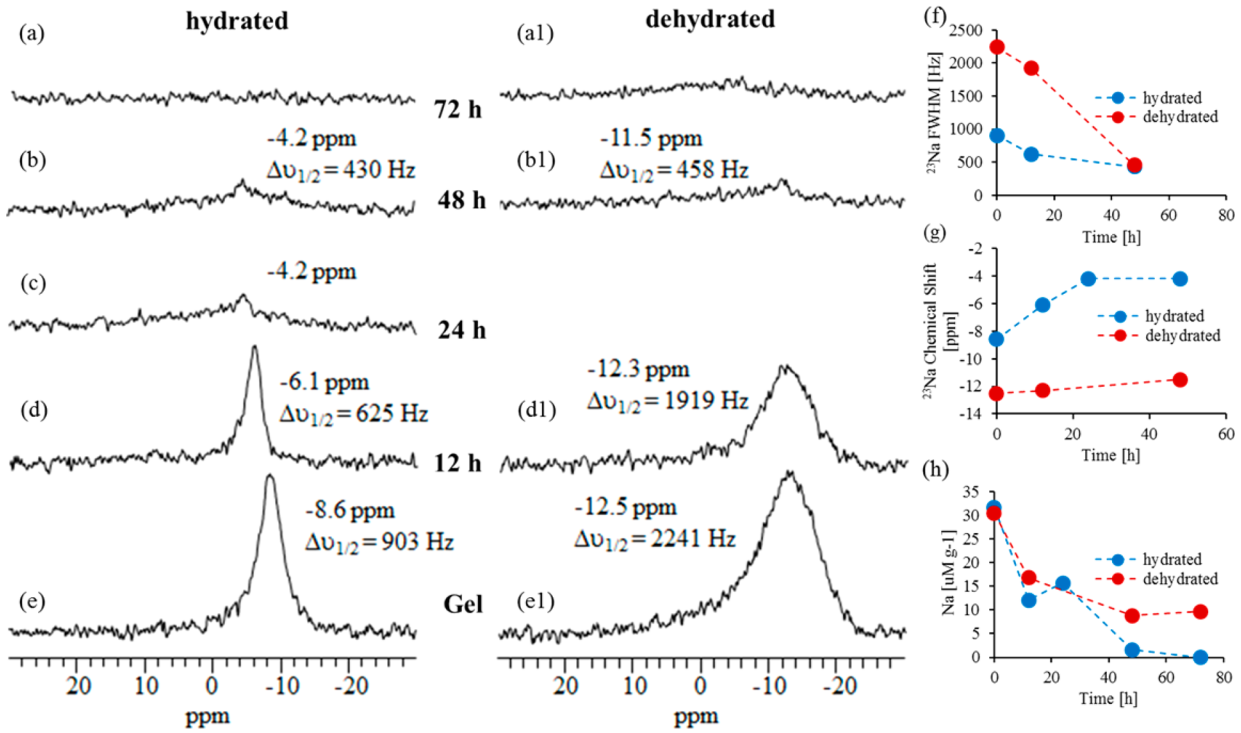

Figure 6. ^{23}Na MAS NMR spectra and spectral analysis for solids extracted from the synthesis process of converting gel to gibbsite at various reaction times, before (a-e) and after dehydration (a1−e1). The gel is shown in spectra a and a1, the 12 h product is shown in spectra b and b2, the 24 h product is shown in spectrum c, the 48 h product is shown in spectra d and d1, and the 72 h product is shown in spectra e and e1. Graphs of the line width (f), chemical shift (g), and loading (i) of the ^{23}Na spectra are also included.

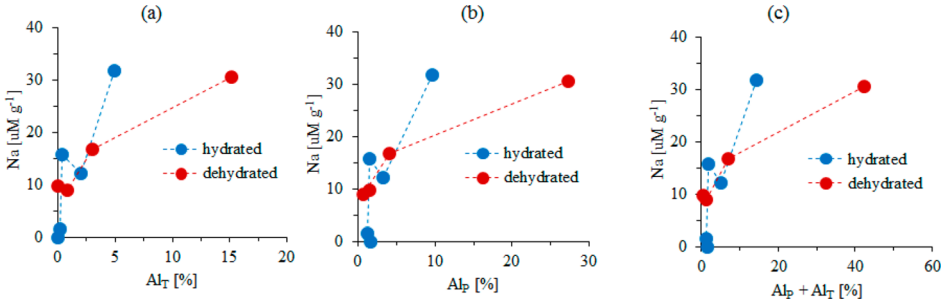

Figure 7. Correlation between the concentration of Na and those of Al_T (a), Al_P (b), and Al_T + Al_P (c), respectively, on the hydrated (blue) and the dehydrated (red) solid samples from the conversion of gel to gibbsite using the data from Figures 1 and 6.

with increasing reaction time appears to correlate with the commensurate increase in the surface-to-volume ratio as the gibbsite crystal size increases (cf., Figure 5), resulting in a decreased number of Na cations in the system per sample mass (Figure S2). Given this apparent systematic relationship between Na concentration and increasing reaction time, the Na content is most likely present as surface species. The role of Na at the gibbsite surface during growth is unclear, but it could range from spectator ion adsorbed as a simple residual from the solution phase to an active participant in the polymerization and condensation of aluminate ions at the gibbsite/solution interface. To address the question whether or not Na might be directly associated with Al_T or Al_P sites, the apparent surface concentration of penta- and tetra-coordinated Al sites is quantitatively compared with the apparent surface concentration of Na at each reaction time of gel−gibbsite synthesis. A positive correlation is obtained between the amount of Al_T or Al_P sites or both Al_T and Al_P (Figure 7, parts a, b, and c, respectively). It appears that Na preferentially binds at defect sites at the surface, which comprises under-coordinated Al centers.

CONCLUSIONS

Single-pulse ^{27}Al and ^{23}Na MAS NMR measurements conducted on solid samples extracted during the crystallization of gibbsite from an amorphous gel precursor enabled quantitative characterization of Al coordination sites through this transformation and determination of their probable location along with Na on the surface of gibbsite nanoplates. The use of a high field of 19.975 T and a moderate sample spinning rate of 20 kHz allowed trace low-coordinated Al_T and Al_P species to be quantified alongside fully coordinated Al_O. Because the peaks for these three species were well-resolved in the ^{27}Al MAS NMR spectrum, low-coordinated Al sites with percentages as low as 0.1% of the total Al sites could be detected. The following results were obtained: (a) Al_T and Al_P coexist but gradually diminish in concentration from that in the amorphous gel precursor as crystalline gibbsite nucleates and

DOI: 10.1021/acs.jpcc.7b10424
J. Phys. Chem. C 2017, 121, 27555−27562

grows, yielding final percentages of less than 1% for the primary synthesis protocol evaluated. (b) Different synthesis methods can generate gibbsite samples with varying amounts of these under-coordinated Al sites. (c) The amorphous gel precursor contains a substantial amount of these low-coordinated Al sites to begin with, at an A_O:Al_P:Al_T ratio of approximately 4:2:1. (d) In the presence of water, the low-coordinated Al sites on solid surfaces become octahedrally coordinated by binding with the oxygen atom in H_2O, and their ^{27}Al MAS NMR peaks shift to the location of the Al_O sites, while internal under-coordinated Al sites remain unaffected. (e) Gibbsite crystallization involves converting Al_P and Al_T sites into Al_O sites. (f) Co-associated Na cations reside as surface-associated sorbates on the final gibbsite product. These findings help provide a basis for constructing a mechanistic model for gibbsite crystallization, a model that ultimately is required to predict and control gibbsite precipitation and dissolution at the industrial processing scale.

■ ASSOCIATED CONTENT

Supporting Information

The Supporting Information is available free of charge on the ACS Publications website at DOI: 10.1021/acs.jpcc.7b10424.

Quadrupolar line parameters, line-fitting, spin-counting, and calculation details (PDF)

■ AUTHOR INFORMATION

Corresponding Authors

*J.Z.H. e-mail: Jianzhi.hu@pnnl.gov.
*K.M.R. e-mail: Kevin.Rosso@pnnl.gov.

ORCID

Jian Zhi Hu: 0000-0001-8879-747X
Nicholas R. Jaegers: 0000-0002-9930-7672
Chuan Wan: 0000-0002-8226-7619
Kevin M. Rosso: 0000-0002-8474-7720

Author Contributions

§J.Z.H. and X.Z. contributed equally to this work, as did N.R.J., C.W., and T.R.G.

Notes

The authors declare no competing financial interest.

■ ACKNOWLEDGMENTS

This work was supported by IDREAM (Interfacial Dynamics in Radioactive Environments and Materials), an Energy Frontier Research Center funded by the U.S. Department of Energy (DOE), Office of Science, Basic Energy Sciences (BES). Materials characterization and NMR measurements were performed using EMSL, a national scientific user facility sponsored by the DOE Office of Biological and Environmental Research and located at Pacific Northwest National Laboratory (PNNL). PNNL is a multiprogram national laboratory operated for DOE by Battelle Memorial Institute under Contract No. DE-AC06-76RLO-1830.

■ REFERENCES

(1) Li, X.-b.; Liu, Z.-j.; Xu, X.-h.; Zhou, Q.-s.; Peng, Z.-h.; Liu, G.-h. Model of Apparent Crystal Growth Rate and Kinetics of Seeded Precipitation from Sodium Aluminate Solution. *J. Cent. South Univ. Technol.* **2005**, *12*, 662−666.

(2) Blanks, K. A. Novel Synthesis of Gibbsite by Laser-Stimulated Nucleation in Supersaturated Sodium Aluminate Solutions. *J. Cryst. Growth* **2000**, *220*, 572−578.

(3) Addai-Mensah, J. Surface and Structural Characteristics of Gibbsite Precepitated from Pure, Synthetic Bayer Liquor. *Miner. Eng.* **1997**, *10*, 81−96.

(4) Herting, D. L.; Reynolds, J. G.; Barton, W. B. Conversion of Coarse Gibbsite Remaining in Hanford Nuclear Waste Tank Heels to Solid Sodium Aluminate [$NaAl(OH)_4 \cdot 1.5H_2O$]. *Ind. Eng. Chem. Res.* **2014**, *53*, 13833−13842.

(5) Reynolds, J. G.; McCoskey, J. K.; Herting, D. L. Gibbsite Solubility in Hanford Nuclear Waste Approached from above and Below Saturation. *Ind. Eng. Chem. Res.* **2016**, *55*, 5465−5473.

(6) Reynolds, J. G. The Apparent Solubility of Aluminum (III) in Hanford High-Level Waste. *J. Environ. Sci. Health, Part A: Toxic/Hazard. Subst. Environ. Eng.* **2012**, *47*, 2213−2218.

(7) Krupka, K. M.; Cantrell, K. J.; Schaef, H. T.; Arey, B. W.; Heald, S. M.; Deutsch, W. J.; Lindberg, M. J. In *Characterization of Solids in Residual Wastes from Single-Shell Tanks at the Hanford Site, Washington, USA - 9277*; Report PNNL-SA-63382; WM Symposia Inc.: Tempe, AZ, 2009.

(8) Gong, X.; Nie, Z.; Qian, M.; Liu, J.; Pederson, L. A.; Hobbs, D. T.; McDuffie, N. G. Gibbsite to Boehmite Transformation in Strongly Caustic and Nitrate Environments. *Ind. Eng. Chem. Res.* **2003**, *42*, 2163−2170.

(9) Xu, T.; Catalano, J. G. Impacts of Surface Site Coordination on Arsenate Adsorption: Macroscopic Uptake and Binding Mechanisms on Aluminum Hydroxide Surfaces. *Langmuir* **2016**, *32*, 13261−13269.

(10) Levin, I.; Brandon, D. Metastable Alumina Polymorphs: Crystal Structures and Transition Sequences. *J. Am. Ceram. Soc.* **1998**, *81*, 1995−2012.

(11) Peskleway, C. D.; Henderson, G. S.; Wicks, F. J. Dissolution of Gibbsite: Direct Observations Using Fluid Cell Atomic Force Microscopy. *Am. Mineral.* **2003**, *88*, 18.

(12) Bickmore, B. R.; Tadanier, C. J.; Rosso, K. M.; Monn, W. D.; Eggett, D. L. Bond-Valence Methods for Pka Prediction: Critical Reanalysis and a New Approach. *Geochim. Cosmochim. Acta* **2004**, *68*, 2025−2042.

(13) Kinsey, R. A.; Kirkpatrick, R. J.; Hower, J.; Smith, K. A.; Oldfield, E. High Resolution Aluminum-27 and Silicon-29 Nuclear Magnetic Resonance Spectroscopic Study of Layer Silicates, Including Clay Minerals. *Am. Mineral.* **1985**, *70*, 537.

(14) Isobe, T.; Watanabe, T.; d'Espinose de la Caillerie, J. B.; Legrand, A. P.; Massiot, D. Solid-State ^{1}H and ^{27}Al NMR Studies of Amorphous Aluminum Hydroxides. *J. Colloid Interface Sci.* **2003**, *261*, 320−324.

(15) Okumura, M.; Sassi, M.; Rosso, K. M.; Machida, M. Origin of 6-Fold Coordinated Aluminum at (010)-Type Pyrophyllite Edges. *AIP Adv.* **2017**, *7*, 055211.

(16) Qian, Z.; Feng, H.; Jin, X.; Yang, W.; Wang, Y.; Bi, S. Density Functional Investigation of the Water Exchange Reaction on the Gibbsite Surface. *Environ. Sci. Technol.* **2009**, *43*, 9281−9286.

(17) Sipos, P. The Structure of Al(III) in Strongly Alkaline Aluminate Solutions — a Review. *J. Mol. Liq.* **2009**, *146*, 1−14.

(18) Kwak, J. H.; Hu, J.; Lukaski, A.; Kim, D. H.; Szanyi, J.; Peden, C. H. F. Role of Pentacoordinated Al^{3+} Ions in the High Temperature Phase Transformation of Γ-Al_2O_3. *J. Phys. Chem. C* **2008**, *112*, 9486−9492.

(19) Neuville, D. R.; Cormier, L.; Massiot, D. Al Environment in Tectosilicate and Peraluminous Glasses: A ^{27}Al MQ-MAS NMR, Raman, and XANES Investigation. *Geochim. Cosmochim. Acta* **2004**, *68*, 5071−5079.

(20) MacKenzie, K. J. D.; Smith, M. E. *Multinuclear Solid-State NMR of Inorganic Materials*; Pergamon: New York, 2002.

(21) Sugiyama, K.; Shinohara, A. H.; Saito, F.; Waseda, Y. Study on Dry Grinding of Gibbsite (Hydrargillite). *Mineral. J.* **1994**, *17*, 101−110.

(22) Kao, H.-M.; Wu, R.-R.; Chen, T.-Y.; Chen, Y.-H.; Yeh, C.-S. Probing the Formation Process of Aluminium Hydroxide Nanoparticles Prepared by Laser Ablation with Al NMR Spectroscopy. *J. Mater. Chem.* **2000**, *10*, 2802−2804.

DOI: 10.1021/acs.jpcc.7b10424
J. Phys. Chem. C 2017, 121, 27555−27562

(23) Vyalikh, A.; Massiot, D.; Scheler, U. Structural Characterisation of Aluminium Layered Double Hydroxides by ^{27}Al Solid-State NMR. *Solid State Nucl. Magn. Reson.* **2009**, *36*, 19−23.
(24) Bradley, S. M.; Hanna, J. V. ^{27}Al and ^{23}Na MAS NMR and Powder X-Ray Diffraction Studies of Sodium Aluminate Speciation and the Mechanistics of Aluminum Hydroxide Precipitation Upon Acid Hydrolysis. *J. Am. Chem. Soc.* **1994**, *116*, 7771−7783.
(25) Shen, S.; Chow, P. S.; Chen, F.; Feng, S.; Tan, R. B. H. Synthesis of Submicron Gibbsite Platelets by Organic-Free Hydrothermal Crystallization Process. *J. Cryst. Growth* **2006**, *292*, 136−142.
(26) Louaer, S.; Wang, Y.; Guo, L. Fast Synthesis and Size Control of Gibbsite Nanoplatelets, Their Pseudomorphic Dehydroxylation, and Efficient Dye Adsorption. *ACS Appl. Mater. Interfaces* **2013**, *5*, 9648−9655.
(27) Hu, J. Z.; et al. High Field Al-27 MAS NMR and TPD Studies of Active Sites in Ethanol Dehydration Using Thermally Treated Transitional Aluminas as Catalysts. *J. Catal.* **2016**, *336*, 85−93.
(28) Kwak, J. H.; Hu, J. Z.; Mei, D.; Yi, C. W.; Kim, D. H.; Peden, C. H. F.; Allard, L. F.; Szanyi, J. Coordinatively Unsaturated Al^{3+} Centers as Binding Sites for Active Catalyst Phases of Platinum on Gamma-Al_2O_3. *Science* **2009**, *325*, 1670−1673.
(29) Vyalikh, A.; Zesewitz, K.; Scheler, U. Hydrogen Bonds and Local Symmetry in the Crystal Structure of Gibbsite. *Magn. Reson. Chem.* **2010**, *48*, 877−881.
(30) Hu, J. Z.; Wan, C.; Vjunov, A.; Wang, M.; Zhao, Z.; Hu, M. Y.; Camaioni, D. M.; Lercher, J. A. ^{27}Al MAS NMR Studies of HBEA Zeolite at Low to High Magnetic Fields. *J. Phys. Chem. C* **2017**, *121*, 12849−12854.
(31) Zhao, Z. C.; Xu, S. C.; Hu, M. Y.; Bao, X. H.; Peden, C. H. F.; Hu, J. Z. Investigation of Aluminum Site Changes of Dehydrated Zeolite H-Beta During a Rehydration Process by High-Field Solid-State NMR. *J. Phys. Chem. C* **2015**, *119*, 1410−1417.

DOI: 10.1021/acs.jpcc.7b10424
J. Phys. Chem. C 2017, 121, 27555−27562